0026-895X/11/8004-573–584$25.00
MOLECULAR PHARMACOLOGY
Vol. 80, No. 4
73460/3714042
Mol Pharmacol 80:573–584, 2011
Printed in U.S.A.

Interactions of Key Charged Residues Contributing to Selective Block of Neuronal Sodium Channels by μ-Conotoxin KIIIA[S]

J. R. McArthur, G. Singh, D. McMaster, R. Winkfein, D. P. Tieleman, and R. J. French

Department of Physiology and Pharmacology, and the Hotchkiss Brain Institute (J.R.M., D.M., R.W., R.J.F.), and Department of Biological Sciences and the Institute of Biocomplexity and Informatics (G.S., D.P.T.), University of Calgary, Calgary, Alberta, Canada

Received May 16, 2011; accepted June 27, 2011

ABSTRACT

Voltage-gated sodium channels are important in initiating and propagating nerve impulses in various tissues, including cardiac muscle, skeletal muscle, the brain, and the peripheral nerves. Hyperexcitability of these channels leads to such disorders as cardiac arrhythmias ($Na_v1.5$), myotonias ($Na_v1.4$), epilepsies ($Na_v1.2$), and pain ($Na_v1.7$). Thus, there is strong motivation to identify isoform-specific blockers and the molecular determinants underlying their selectivity among these channels. μ-Conotoxin KIIIA blocks $rNa_v1.2$ (IC_{50}, 5 nM), $rNa_v1.4$ (37 nM), and $hNa_v1.7$ (97 nM), expressed in mammalian cells, with high affinity and a maximal block at saturating concentrations of 90 to 95%. Mutations of charged residues on both the toxin and channel modulate the maximal block and/or affinity of KIIIA. Two toxin substitutions, K7A and R10A, modulate the maximal block (52–70%). KIIIA-H12A and R14A were the only derivatives tested that altered Na_v isoform specificity. KIIIA-R14A showed the highest affinity for $Na_v1.7$, a channel involved in pain signaling. Wild-type KIIIA has a 2-fold higher affinity for $Na_v1.4$ than for $Na_v1.7$, which can be attributed to a missing outer vestibule charge in domain III of $Na_v1.7$. Reciprocal mutations $Na_v1.4$ D1241I and $Na_v1.7$ I1410D remove the affinity differences between these two channels for wild-type KIIIA without affecting their affinities for KIIIA-R14A. KIIIA is the first μ-conotoxin to show enhanced activity as pH is lowered, apparently resulting from titration of the free N terminus. Removal of this free amino group reduced the pH sensitivity by 10-fold. Recognition of these molecular determinants of KIIIA block may facilitate further development of subtype-specific, sodium channel blockers to treat hyperexcitability disorders.

Introduction

Voltage-gated sodium (Na_v) channels are important in the initiation and propagation of nerve impulses in neurons and muscle (Hille, 2001). To date, nine mammalian Na_v channels have been described ($Na_v1.1$–1.9) (Catterall et al., 2005; Al-Sabi et al., 2006); these have differing distributions throughout the body. Gain-of-function mutations in Na_v channels causing hyperexcitability, have been linked to such disease states as cardiac arrhythmia (Wang et al., 1995), epilepsy (Escayg et al., 2000), myotonia (Cannon, 1997), and pain (Waxman et al., 1999). Thus, there is much interest in producing subtype-selective blockers of specific Na_v channel isoforms.

Venoms from fish-hunting cone snails contain many different toxins, which represent possible therapeutic compounds targeting various ion channels. μ-Conotoxins (μCTXs) make up one such group of toxins. As a group, μCTXs are identified by their conserved disulfide backbone structure and because they all target toxin site 1, in the outer pore vestibule, of Na_v channels (Catterall et al., 2005). μCTXs from different species target various Na_v channels and show differing selectivity profiles. μCTX GIIIA from *Conus geographus* specifically targets skeletal muscle channels ($Na_v1.4$) (Cruz et al., 1985), whereas the very similar μCTX, PIIIA, from *Conus purpurascens* most strongly inhibits skeletal muscle channels but also blocks some neuronal channels ($Na_v1.2$ and $Na_v1.7$) with lower affinity (Shon et al., 1998).

μCTX KIIIA, from *Conus kinoshitai*, points to the potential importance of μCTXs as possible therapeutic compounds by showing analgesic activity (Zhang et al., 2007). KIIIA is the shortest known μCTX, at only 16 amino acids in length, but retains the typical μCTX disulfide bond pattern (Bulaj et al., 2005) (Fig. 1). KIIIA has a nominal net charge of +4, lower than both GIIIA (+6) and PIIIA (+7). It is noteworthy that KIIIA was the first μCTX to show higher affinity for the

This work was supported by the Canadian Institutes of Health Research [Grants MOP-10053, MOP-62690]; and the Heart and Stroke Foundation of Alberta, NWT, and Nunavut.

Article, publication date, and citation information can be found at http://molpharm.aspetjournals.org.

doi:10.1124/mol.111.073460.

[S] The online version of this article (available at http://molpharm.aspetjournals.org) contains supplemental material.

ABBREVIATIONS: Na_v, voltage-gated sodium channel; μCTX, μ-conotoxin; GIIIA, μ-conotoxin GIIIA; PIIIA, μ-conotoxin PIIIA; HPLC, high-performance liquid chromatography; HEK, human embryonic kidney; PCR, polymerase chain reaction; MD, molecular dynamics.

neuronal channel, $Na_v1.2$, than for skeletal muscle channels (Zhang et al., 2007). Indeed, KIIIA block of $Na_v1.2$ is almost irreversible on a normal experimental time scale. KIIIA also shows a high affinity (IC_{50} in the nanomolar range) for $Na_v1.7$, a channel involved in pain perception (Yang et al., 2004).

Unlike μCTXs studied previously, KIIIA does not block 100% of the single-channel current (Zhang et al., 2007). This residual single-channel current may be permitted by the absence of arginine and lysine residues in its N-terminal segment (residues 1–6), given that the PIIIA R12A derivative shows a small residual current similar to that for KIIIA (McArthur et al., 2011a). Even though KIIIA binds to the sodium-channel pore site 1, either tetrodotoxin or saxitoxin can bind simultaneously (Zhang et al., 2009), increasing the range of possible pharmacological actions of KIIIA by its use in combination with the smaller pore blockers.

Here we examine differences in binding, resulting from charge-neutralizing substitutions in KIIIA, for $Na_v1.2$ (central nervous system), $Na_v1.4$ (skeletal muscle), and $Na_v1.7$ (peripheral nervous system). Channel mutants were selected based on sequence comparisons (Fig. 1B) and previous docking simulations of μCTXs GIIIA and PIIIA (Choudhary et al., 2007; McArthur et al., 2011a). We focused on two positions: 1) the outer ring charge in domain III, which is absent in $Na_v1.7$ but present in $Na_v1.4$ and $Na_v1.2$; and 2) the aromatic residue in domain I, adjacent to the DEKA locus, which has important implications for tetrodotoxin and saxitoxin block (Santarelli et al., 2007) and thus could be important in KIIIA block. These residues distinguish the canonical μCTX target, $Na_v1.4$, from the neuronal channels $Na_v1.2$ and $Na_v1.7$. We tested the effects of changes at these loci to find how they might contribute to the observed selectivity of KIIIA among the different channel isoforms.

We show that, by substitution of individual KIIIA residues, or by altering the extracellular pH, we can change key features of KIIIA block, including maximal block, affinity and targeting selectivity. Two residues, Lys7 and Arg10, are key determinants of KIIIA's fractional block of single-channel currents, or of maximal conductance in whole-cell experiments. KIIIA's affinity, for all three Na_v channels studied, increased with a decrease in extracellular pH based on increases in the toxin association rates. The increased affinity at low pH can be mostly attributed to titration of KIIIA's free N terminus. By comparison, PIIIA, with a neutral, cyclized pyroglutamate as its N-terminal residue, shows no substantial pH dependence. Changes in channel isoform targeting were seen for the KIIIA-R14A derivative, which showed 10-fold selectivity for $Na_v1.7$, a channel involved in the pain pathway (Yang et al., 2004; Cox et al., 2006), over $Na_v1.2$ and $Na_v1.4$. These molecular determinants of μCTX-selective targeting, offer clues to the design of more selective blockers of tissue-specific Na_v channel isoforms.

A

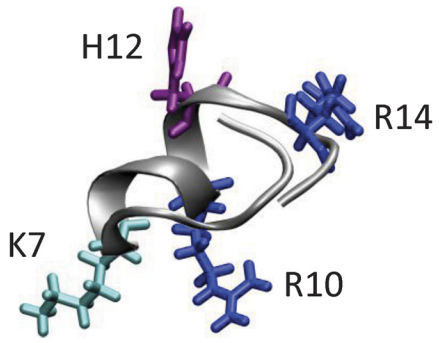

				1	2	3	–	–	–	–	4	5	6	7	8	9	10	11	12	13	14	15	16	
KIIIA				C	C	N	–	–	–	–	C	S	S	K	W	C	R	D	H	S	R	C	C*	
GIIIA		1-R	D	C	C	T	O	O	K	K	C	K	D	R	Q	C	K	O	Q	–	R	C	C	A*-22
PIIIA	pE	R	L	C	C	G	F	O	K	S	C	R	S	R	Q	C	K	O	H	–	R	C	C*	
	1	2	3	4	5	6	7	8	9	10	11	12	13	14	15	16	17	18	19	–	20	21	22	

B

		Inner Ring							Outer Ring							
Domain I P-loop																
$Na_v1.2$	378	–	–	–	–	–	–	F	–	–	–	–	Y	–	–	– 393
$Na_v1.4$	394	F	R	L	M	T	Q	D	Y	W	E	N	L	F	Q	L T 409
$Na_v1.7$	355	–	–	–	–	–	–	–	–	–	–	–	Y	–	Q	– 370
$Na_v1.4$ Y401F		–	–	–	–	–	–	F	–	–	–	–	–	–	–	–
Domain III P-loop																
$Na_v1.2$	1416	–	–	–	–	–	–	–	–	–	–	–	–	–	–	– 1431
$Na_v1.4$	1231	L	Q	V	A	T	F	K	G	W	M	D	I	M	Y	A A 1246
$Na_v1.7$	1400	–	–	–	–	–	–	–	–	–	T	I	–	–	–	– – 1415
$Na_v1.4$ D1241I		–	–	–	–	–	–	–	–	–	–	I	–	–	–	– –
$Na_v1.7$ I1410D		–	–	–	–	–	–	–	–	–	T	D	–	–	–	– –

Fig. 1. Model of KIIIA structure. A, structure of KIIIA (coordinates kindly provided by Drs. Brian Smith and Ray Norton) with important residues highlighted (Lys7, cyan; Arg10/Arg14, blue; His12, purple). B, sodium-channel sequence alignment of the domains I and III p-loop regions, with inner ring (blue) and outer ring (red) labeled. Sequences of channel mutants $rNa_v1.4$ Y401F, $rNa_v1.4$ D1241I, and $hNa_v1.7$ D1241I are shown.

Materials and Methods

Toxin Synthesis and Preparation. Conotoxin synthesis, purification, and disulfide bond formation were performed as described previously in detail (Hui et al., 2002). In brief, linear peptides were synthesized by solid-phase synthesis using 9-flurenylmethoxycarbonyl chemistry. Coupling of 9-flurenylmethoxycarbonyl amino acids was performed using the 1-hydroxybenzotriazole/2-(1*H*-benzotriazol-1-yl)-1,1,3,3-tetramethyluronium hexafluorophosphate/*N*,*N*-diisopropylethylamine method on a Quartet Synthesizer (Protein Technologies Inc., Tucson, AZ).

Crude linear peptide was subjected to oxidative folding under equilibrating condition (i.e., air oxidation in ammonium acetate buffer, pH ~7.6, in the presence of a small amount of mercaptoethanol (10 μl in 150 ml) to promote the formation of the most stable disulfide bonds. During oxidization, the cyclization of the peptide was monitored by analytical HPLC, which was completed in 2 to 4 days at 4°C. The crude cyclized peptide showed a single major peak on analytical HPLC, with some minor peaks being seen in each case (the number and size of minor peaks varied with the derivative being cyclized). The crude cyclized peptide was then isolated from the acidified reaction mixture by reversed-phase extraction, was purified to near homogeneity by HPLC, and the identity of the purified peptide was confirmed by matrix-assisted laser desorption ionization mass spectrometric molecular weight determination. Some derivatives produced two separate peaks, and thus the peak identified as active by Zhang et al. (2007) was used.

Lyophilized conotoxin derivatives were then dissolved in the bath solution to an appropriate stock concentration. Toxin solutions used in the experiments were further diluted in the bath solution to the required concentration.

Sodium Channel Expression in HEK293 Cells. Mammalian expression plasmids encoding rNa$_v$1.2 (pCDM8, a gift from W. A. Catterall) (Linford et al., 1998), rNa$_v$1.4 (pcDNA3.1) (Trimmer et al., 1989), and hNa$_v$1.7 (pCMV6) (Hildebrand et al., 2011) were used. Channel constructs were created using rNa$_v$1.4 or hNa$_v$1.7 as a template. Three channel mutants (rNa$_v$1.4 Y401F, rNa$_v$1.4 D1241I, and hNa$_v$1.7 I1410D) were constructed. In brief, sense and antisense primers encoding point mutations for the desired amino acid substitution were synthesized and used in high-fidelity PCRs (Phusion polymerase; Thermo Fisher Scientific, Waltham, MA) with primers located either 3′ or 5′, respectively, from unique flanking restriction sites in the wild-type construct. Amplified fragments (upstream and downstream) were run on agarose gels, and the resulting products were isolated, mixed, and subjected to another round of high-fidelity PCR using only the 3′ and 5′ primers. The resulting product was purified, digested with the appropriate restriction endonucleases, and cloned into like-digested wild-type channel clones. All fragments cloned from PCR products were completely sequenced to ensure no PCR-generated misincorporations had occurred during cloning.

HEK293 cells were transiently cotransfected with the plasmid encoding the particular sodium channel α-subunit (2 μg) and a plasmid encoding green fluorescent protein (0.5 μg), allowing transfected cells to be identified by their green fluorescence. Twenty-four hours after transfection, cells were plated on to coverslips and used for voltage-clamp studies at least 2 h after plating.

Electrophysiology. Sodium channel currents were recorded by the patch-clamp technique in the whole-cell configuration at room temperature (23–25°C). The bath solution contained 140 mM NaCl, 5 mM KCl, 2 mM $CaCl_2$, 1 mM $MgCl_2$, 10 mM HEPES, and 10 mM glucose, adjusted to pH 6, 7.4, or 9 with HCl or NaOH (~305 mOsmol/kg). The pipette electrodes had a final tip resistance of 1 to 3 MΩ with an internal solution composed of 35 mM NaCl, 105 mM CsF, 1 mM $MgCl_2$, 10 mM HEPES, and 1 mM EGTA, with pH adjusted to 7.2 with CsOH (~295 mOsmol/kg).

Whole-cell patch clamp was performed with an EPC7 Amplifier (HEKA, Lambrecht/Pfalz, Germany). Current traces were filtered at 3 kHz (low-pass, three-pole Bessel filter, EPC7) and sampled at 200 kHz using pClamp9.2 software (Molecular Devices, Sunnyvale, CA), with series resistance compensated typically at 40 to 60%. Cells showing peak currents between 0.5 and 5 nA were used to ensure adequate voltage control while maintaining good current resolution. Toxins were then locally superfused over the cell at a rate of 10 to 20 μl/min (bath volume of 5 ml). Currents were elicited with a 2-s prepulse to −140 mV to remove inactivation followed by a test pulse to −10 mV for 10 ms repeated every 5 s during toxin application and washout to record kinetics. Single-channel bilayer experiments using batrachotoxin-modified skeletal muscle Na$_v$ channel at steady state were carried out as described previously (McArthur et al., 2011a).

Data Analysis. Each point data point on a dose-response curve was from data for one toxin-containing solution applied to a single cell, with control data taken before and after toxin application on the same cell. Overall, 27 dose-response curves were generated using 6 different channel constructs, and 6 toxin derivatives, with 18 ± 4 experiments contributing to each dose-response curve. Typically three to four determinations were done at each concentration (range, 1–9). Dose-response curves are plotted as the estimated fraction of channels blocked $Fb_{ss} = (1 - I_{tx}/I_{ctr})$ versus concentration of toxin, where I_{tx} is the residual current in the presence of the toxin at steady state and I_{ctr} is the current level before toxin application. Data were fit with a rectangular hyperbola, assuming a Hill coefficient of 1, using the following expression, where IC_{50} is the toxin concentration for half-maximal inhibition. Here, Fb_{ss} is the fraction of current blocked by the toxin at steady state, at a particular concentration, and Fb_{sc} represents the maximal fraction of current blocked at saturating concentrations of the toxin (and the fractional block of the single-channel current). The parameters Fb_{sc} and IC_{50} were varied to obtain the best fit.

$$Fb_{ss} = \frac{Fb_{sc}}{1 + \frac{IC_{50}}{[tx]}}$$

Toxin blocking kinetics (k_{on} and k_{off}) were measured by fitting the peak currents for successive depolarizations during toxin wash-in or wash-out test with a single exponential to determine τ_{on} and τ_{off}. The rates constants, k_{on} and k_{off}, and the equilibrium dissociation constant, K_d (Fig. 2, A and B) were calculated using the following equations:

$$k_{on} = \frac{Fb_{ss}/Fb_{sc}}{\tau_{on} \cdot [tx]} \quad k_{off} = \frac{1}{\tau_{off}} \quad K_d = \frac{k_{off}}{k_{on}}$$

For ease of reading in the text, group data are represented as mean values, with full statistics provided in the tables. Differences between group data sets were considered significant if $p < 0.05$ in an unpaired t test, unless otherwise stated.

Molecular Dynamics Simulations. Molecular dynamics (MD) simulations of the docking of μCTX KIIIA (Bulaj et al., 2005) to a sodium channel model (Choudhary et al., 2007) were performed as described previously (McArthur et al., 2011b). In brief, MD simulations were carried out using the GROMACS set of programs (Berendsen et al., 1984; Lindahl et al., 2001) using the AMBER 99 force field. At first, KIIIA was superposed on to the docked structure of GIIIA. Ten simulations of 20 ns were run, and the resulting structures were aligned with respect to the channel backbone using a least-squares fit and clustered using the g_cluster program (Daura et al., 1999), with a root mean square deviation cutoff of 0.4 nm. The top cluster incorporated >60% (2818) of all the structures (4501), and the center of the cluster was chosen to represent the toxin-bound conformation. All visualization of molecules was carried out using visual MD (Humphrey et al., 1996).

Results

Charged residues play critical roles in defining how μCTXs target and block Na$_v$ channels. Despite KIIIA being shorter than both PIIIA and GIIIA, the charged residues in the C-terminal segment are highly conserved across the three toxins despite their differences in Na$_v$ channel selectivity (Fig. 1). To identify residues that might be involved in iso-

form selectivity, we neutralized all basic residues in KIIIA by replacing them with alanines (KIIIA-K7A, R10A, H12A, and R14A) and synthesized a KIIIA derivative, which lacks the N-terminal charge (KIIIA-DA, des-amino). Whole-cell voltage-clamp recordings were used to determine the kinetics of toxin block of $Na_v1.2$, 1.4, and 1.7. The toxin substitutions altered toxin binding and unbinding kinetics, as well as the maximal block at saturating toxin concentrations, to varying

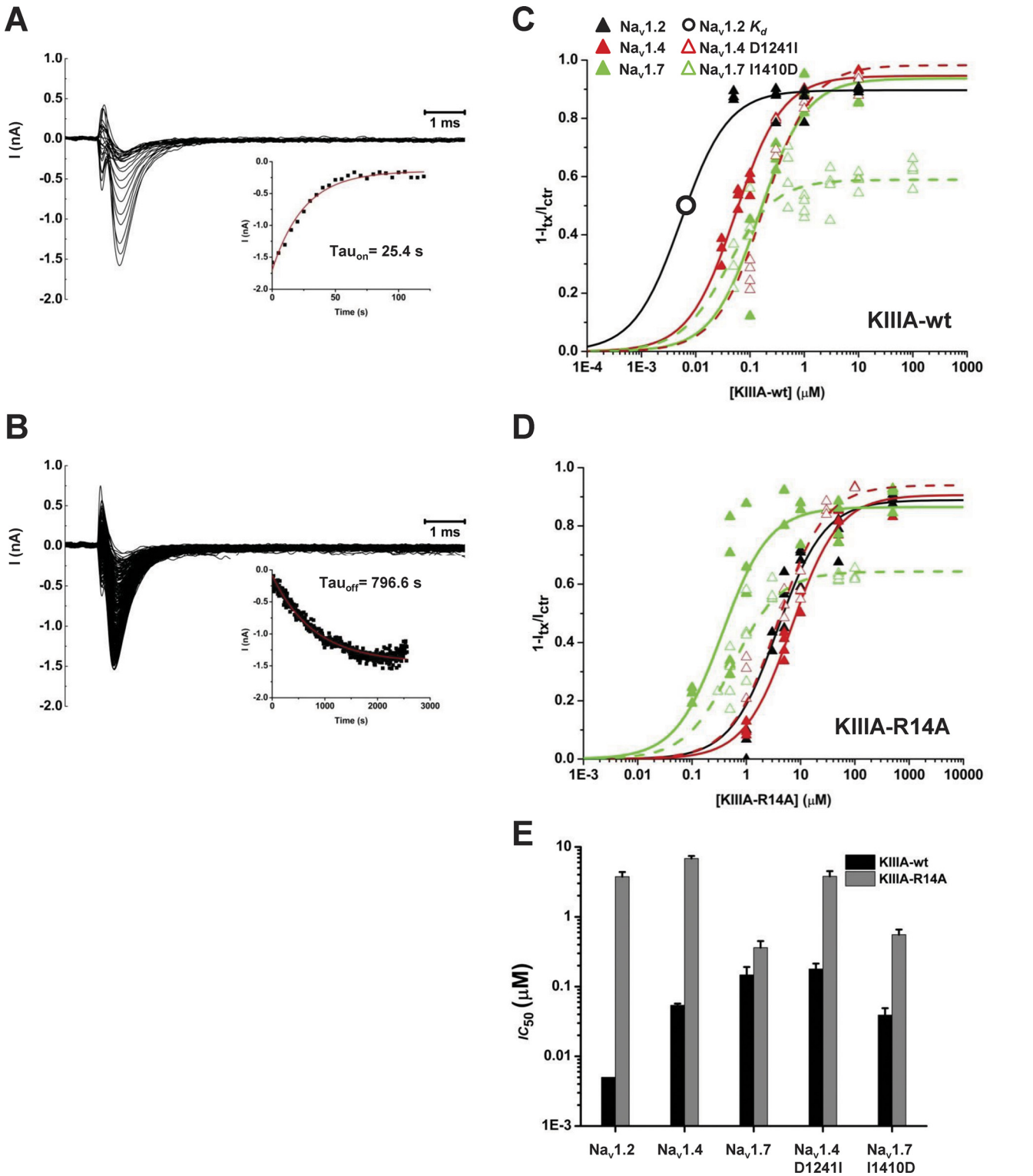

Fig. 2. KIIIA-R14A selectivity profile is altered compared with KIIIA-wt. A, example experiment of KIIIA-wt (1 μM) wash-in in $Na_v1.4$. B, example washout experiment of KIIIA-wt (1 μM) from same cell as A. C and D, dose-response curves for KIIIA-wt (data from 96 cells) and KIIIA-R14A (data from 96 cells) in $Na_v1.2$, $Na_v1.4$, $Na_v1.7$, $Na_v1.4$ D1241I, and $Na_v1.7$ I1410D, respectively. Note that the curve for $Na_v1.2$ and KIIIA-wt in part C, was forced through the kinetically determined K_d (○), because the time constant block was too long near this concentration to reliably attain steady-state block. In other cases, both IC_{50} and the maximal saturating block, Fb_{sc} were determined directly from fits to the steady-state dose-response data. E, comparison of IC_{50} values for KIIIA-wt and KIIIA-R14A in each channel.

degrees in the three channel subtypes. To assess the importance of differences among the channels, we used the following constructs: $Na_v1.4$ Y401F, $Na_v1.4$ D1241I, and $Na_v1.7$ I1410D. These represented the major differences, among the three channels, located near the inner and outer ring charges (Fig. 1B). Unlike previous studies with the larger μCTX GIIIA (Li et al., 2001, 2003; Cummins et al., 2002), which found residues in the domain II turret region to be important in toxin selectivity, we focused on residue differences around the inner and outer ring residues, in part because of KIIIA's smaller size and lower net charge.

Block of $Na_v1.2$, 1.4, and 1.7 by Wild-Type KIIIA. Channel isoforms $Na_v1.2$, 1.4, and 1.7 were expressed heterologously in HEK293 cells, and currents were recorded using the whole-cell patch-clamp technique at pH 7.4. Kinetics of block by KIIIA-wt were determined from whole-cell currents elicited by repeated depolarizing steps (Fig. 2, A and B). KIIIA blocked $Na_v1.2$ with the highest affinity (K_d = 5 nM) compared with $Na_v1.4$ (K_d = 37 nM) and $Na_v1.7$ (K_d = 97 nM) (Table 1). Dose-response curves are plotted in Fig. 2C. As shown in the dose-response curves, all three channels showed similar maximal block levels ($Na_v1.2$, 90%; $Na_v1.4$, 95%; and $Na_v1.7$, 94%) at saturating concentrations of wild-type KIIIA. Kinetics are very slow in $Na_v1.2$, making it impractical to collect truly steady-state data. Thus, this dose-response curve was fit using an IC_{50} of 5 nM, equal to the kinetically determined K_d. Other cases provided steady-state data, which allowed direct determination of IC_{50} values from the dose-response relation, and these values correspond well with K_d, values determined from the kinetics. Overall, wild-type KIIIA (KIIIA-wt) shows a range of binding affinities of ~30-fold in the following order: $Na_v1.2 > Na_v1.4 > Na_v1.7$ (IC_{50}/K_d values: 5, 54, and 147 nM, respectively).

The underlying differences in binding and unbinding kinetics are shown in Table 1. $Na_v1.2$ and $Na_v1.7$ had slow association rates, k_{on} (0.28 and 0.18 $\mu M^{-1} \cdot min^{-1}$, respectively) relative to that of $Na_v1.4$ (1.6 $\mu M^{-1} \cdot min^{-1}$). The dissociation rate constants, k_{off}, also differed among channel isoforms with $Na_v1.2$ being the slowest (0.002 min^{-1}) followed by $Na_v1.7$ (0.017 min^{-1}) with $Na_v1.4$ being the fastest (0.060 min^{-1}). These indicate that the toxin-channel complex has a longer mean lifetime for the neuronal channels, $Na_v1.2$ and $Na_v1.7$, than for the skeletal muscle isoform, $Na_v1.4$. These relationships are reminiscent of previously reported data from studies in *Xenopus laevis* oocytes (Zhang et al., 2007). Despite the skeletal muscle targeting for which the μCTX family is named, KIIIA shows its highest affinity for the brain channel $Na_v1.2$.

Substitution R14A in KIIIA Changes Its Target Specificity. Replacement of KIIIA's arginine-14 with alanine removed a basic side chain resulting in the derivative KIIIA-R14A, which is selective for $Na_v1.7$ over both $Na_v1.2$ and $Na_v1.4$ (IC_{50} values 0.36, 3.7, and 6.8 μM, respectively; see Fig. 2D). KIIIA-R14A showed a slightly decreased k_{on} but unchanged k_{off} values (Table 1) in its interaction with $Na_v1.7$ (0.038 $\mu M^{-1} \cdot min^{-1}$ and 0.020 min^{-1}, respectively). In contrast, for $Na_v1.2$ and $Na_v1.7$, there were changes in both k_{on} and k_{off}, with k_{on} getting slower (0.024 and 0.21 $\mu M^{-1} \cdot min^{-1}$ for $Na_v1.2$ and 1.4, respectively), and k_{off} (0.026 and 1.2 min^{-1} for $Na_v1.2$ and 1.4, respectively) getting faster for both. Despite the changes in affinity there were no significant changes in maximal block compared with KIIIA-wt (range, 87–91%; see Table 1). Here, the dramatic result is that the peripheral nerve channel isoform, $Na_v1.7$, becomes the preferred target for KIIIA R14A by a factor of 10- to 20-fold over $Na_v1.2$ and $Na_v1.4$.

Channel Residues in the Domain III Outer Ring Interact with KIIIA-R14A. Two channel mutants were constructed to look at the effects of the domain III outer ring charge on KIIIA-R14A's binding. Based on previous studies of other μ-conotoxins (Choudhary et al., 2007; McArthur et al., 2011a), it seemed likely that KIIIA's Arg14 should interact with residues in domain III and IV near the outer ring charges. To explore the basis for the observed differences we scanned for sequence differences among $Na_v1.2/1.4$ and $Na_v1.7$ in these domains (Fig. 1B). In human $Na_v1.7$, an isoleucine (Ile1410) is present at the "outer ring" position of domain III, taking the place of the aspartate found in all other Na_v channels (Asp1241 in rat $Na_v1.4$). Thus, we constructed two "exchange" mutants, $rNa_v1.4$ D1241I and $hNa_v1.7$ I1410D, to test for possible interactions with Arg14 in KIIIA.

First, we tested KIIIA-wt on both channels to determine whether this exchange could explain the differences in affinity between $Na_v1.4$ and $Na_v1.7$ for KIIIA-wt (Fig. 2C; Table 1). The $Na_v1.4$ D1241I mutation increased the K_d of wild-type KIIIA to 102 nM (close to that of $Na_v1.7$, 97 nM), whereas the $Na_v1.7$ I1410D mutation decreased the K_d to 56 nM (similar to that of $Na_v1.4$, 37 nM). The mutations had opposite effects on the k_{on} and k_{off} rates. The $Na_v1.4$ D1241I mutation slowed the association rate and sped up the disso-

TABLE 1

Kinetic analysis of KIIIA wild-type and R14A binding (k_{on}) and unbinding (k_{off})

Fractional block at saturating toxin concentrations (Fb_{sc}) are determined from the dose-response data in Fig. 2.

Toxin (KIIIA) and Channel	k_{on}	S.E.M.	k_{off}	S.E.M.	K_d	Fb_{sc}	S.E.M.
	$\mu M^{-1} \cdot min^{-1}$		min^{-1}		μM		
wt							
$Na_v1.2$	0.280	0.026	0.002	5.0×10^{-5}	0.005	0.897	0.016
$Na_v1.4$	1.605	0.202	0.060	0.006	0.037	0.946	0.014
$Na_v1.7$	0.180	0.016	0.017	0.004	0.097	0.937	0.059
$Na_v1.4$ D1241I	0.940	0.126	0.096	0.022	0.102	0.982	0.047
$Na_v1.7$ I1410D	0.529	0.056	0.030	0.004	0.056	0.589	0.018
$Na_v1.4$ Y401F	0.859	0.051	0.060	0.004	0.070	0.924	0.031
R14A							
$Na_v1.2$	0.024	0.004	0.026	0.008	1.083	0.889	0.036
$Na_v1.4$	0.209	0.064	1.187	0.109	5.689	0.906	0.020
$Na_v1.7$	0.038	0.004	0.020	0.004	0.511	0.865	0.041
$Na_v1.4$ D1241I	0.221	0.021	0.807	0.060	3.660	0.940	0.040
$Na_v1.7$ I1410D	0.117	0.021	0.091	0.014	0.782	0.643	0.025

ciation rate, compared with KIIIA-wt block of $Na_v1.4$, accounting for the observed lower affinity of the mutant channel. In turn, $Na_v1.7$ I1410D showed an increased association rate, with little change in the dissociation rate, leading to the observed higher affinity of the mutant channel.

Next, we looked at block of the two channel mutants by KIIIA-R14A (Fig. 2D). In both cases compared with KIIIA-R14A's block of native $Na_v1.4$ and $Na_v1.7$, there was little change in the parameters k_{on}, k_{off}, and K_d. The on and off rates for $Na_v1.4$ D1241I were not significantly different from native $Na_v1.4$. The $Na_v1.7$ I1410D mutant showed slightly increased values of both k_{on} and k_{off}. These changes yielded the observed small differences in K_d (3.7 and 5.7 μM between $Na_v1.4$ and $Na_v1.4$ D1241I, and 0.51 and 0.78 μM for $Na_v1.7$ and $Na_v1.7$ I1410D, respectively; see Table 1).

The $Na_v1.4$ D1241I mutation had no effect on the maximal block by KIIIA-wt (98%), but the $Na_v1.7$ I1410D mutation decreased KIIIA-wt's maximal block to 59% (Fig. 2C). With KIIIA-R14A, the $Na_v1.4$ D1241I mutation induced no significant change in maximal block (94%) compared with $Na_v1.4$, whereas the $Na_v1.7$ I1410D decreased the maximal block level to 64% compared with native $Na_v1.7$ (Fig. 2D).

General implications for binding affinity that emerge of these experiments are that 1) the differences of binding of KIIIA-wt among $Na_v1.4$, $Na_v1.7$, and their reciprocal mutants depend on the presence or absence of an interaction between toxin Arg14 and the domain III outer ring aspartate; and 2) the substitution R14A removes this interaction, so that subsequent replacement of the outer ring aspartate has little influence (affinities for each parent channel and its respective mutant are essentially equal; see Fig. 2E).

Substitution K7A Affects Both the Affinity and Maximal Block. Neutralization of lysine-7 in KIIIA lowers the toxin's affinity for all three channel isoforms, but the K7A derivative has the same selectivity profile as KIIIA-wt ($Na_v1.2 > Na_v1.4 > Na_v1.7$) (Fig. 3A). KIIIA-K7A has a similar effect on IC_{50} in all three channels in that it decreases affinity ~30-fold for all three channel isoforms (Tables 1 and 2). The effects on affinity are mostly due to increases in k_{off} (11- to 20-fold), with small decreases in k_{on} (1.5- to 3-fold). Removal of the Lys7 charge decreased the maximal block of the toxin compared with KIIIA-wt. In $Na_v1.2$ the maximal block was 68%, which was larger than both $Na_v1.4$ and $Na_v1.7$ (60 and 58%, respectively) (Fig. 3B). Examining a similar μCTX, PIIIA, a similar decrease in residual current is seen in $Na_v1.2$ compared with $Na_v1.4$ and $Na_v1.7$, at the homologous position (PIIIA-R14A; see Fig. 3, C and D), suggesting a similar bound orientation of this residue.

A Tyrosine/Phenylalanine Substitution in Domain I Modulates the Maximal Block by KIIIA-K7A. From previous studies of μ-conotoxins, we expected that Lys7 would face down into the pore and would interact predominantly with residues in domain I and II. We scanned the pore regions of $Na_v1.2$, 1.4, and 1.7 in these two domains and found that $Na_v1.4$ and $Na_v1.7$ have a conserved tyrosine one residue external to DEKA locus in domain I, whereas $Na_v1.2$ has a phenylalanine at this position. To test for a role for this residue in determining maximal block by KIIIA-K7A in $Na_v1.2$ versus $Na_v1.4$ and 1.7, we generated a $Na_v1.4$ Y401F mutant. The $Na_v1.4$ Y401F mutant showed a maximal block of 69%, significantly larger than $Na_v1.4$ and 1.7 and the same as $Na_v1.2$ (Fig. 3, A and B). When PIIIA-R14A was tested in the $Na_v1.4$ Y401F construct, The

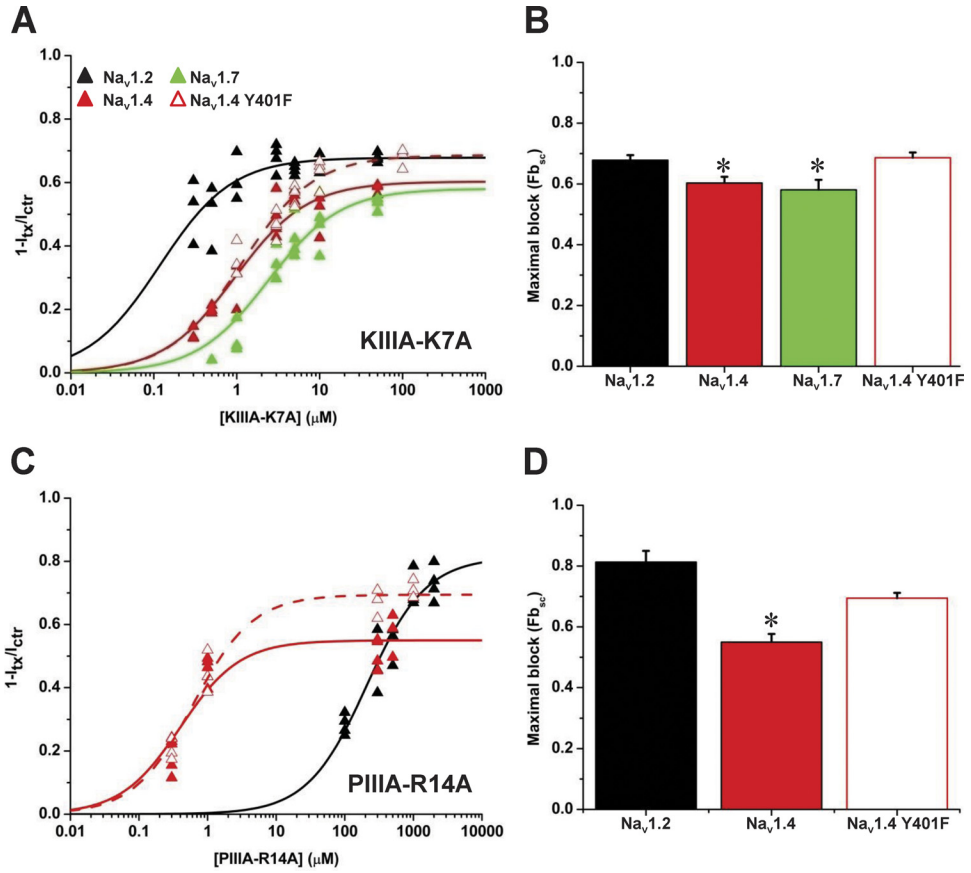

Fig. 3. KIIIA-K7A affects residual current through single channels and is modulated by residues in the pore. A, dose-response curves of KIIIA-K7A (data from 87 cells) in $Na_v1.2$, $Na_v1.4$, $Na_v1.7$, and $Na_v1.4$ Y401F. B, maximal block of ionic current by KIIIA-K7A through $Na_v1.2$, $Na_v1.4$, $Na_v1.7$, and $Na_v1.4$ Y401F. C, dose-response curve of PIIIA-R14A (data from 47 cells) in $Na_v1.2$, $Na_v1.4$, and $Na_v1.4$ Y401F. D, maximal block, by PIIIA-R14A, of ionic current through $Na_v1.2$, $Na_v1.4$, and $Na_v1.4$ Y401F.

residual current was reduced to the same level as the native $Na_v1.2$ residual current level (Fig. 3, C and D). This mutation had little effect on either the IC_{50} values or the kinetics compared with native $Na_v1.4$. In contrast, the $Na_v1.4$ D1241I outer ring mutation did not affect the maximal block by KIIIA-K7A (Supplementary Fig. 1).

Neutral Replacement of Arg10 Decreases Affinity and Maximal Block of KIIIA. Replacement of Arg10 with an alanine in KIIIA increases the IC_{50} of the toxin for all three channel isoforms (~14- to 97-fold) yet retains the KIIIA-wt isoform specificity profile of $Na_v1.2 > Na_v1.4 > Na_v1.7$ (Fig. 4A). The decreases in affinity result from decreases in k_{on} (2- to 4-fold), and increases in k_{off} (3- to 11-fold; see Table 3).

The maximal block of KIIIA-R10A is reduced compared with KIIIA-wt in all three channel isoforms. The largest reduction was seen for $Na_v1.7$, to 52%, whereas reduction of $Na_v1.2$ to 66% and $Na_v1.4$ to 70% showed similar maximal block levels.

We looked at the effects of KIIIA-R10A in the domain III channel mutants, $Na_v1.4$ D1241I and $Na_v1.7$ I1410D. The $Na_v1.4$ D1241I mutant did not significantly affect the IC_{50} of KIIIA-R10A, whereas the $Na_v1.7$ I1410D only slightly increased the IC_{50} (<4-fold). For $Na_v1.4$ D1241I and $Na_v1.7$ I1410D, there were small decreases in both the k_{on} (~2.5-fold) and k_{off} (6-fold), respectively, compared with their respective native channels (Tables 1 and 3). Both channel mutants showed increased maximal block with KIIIA-R10A, to 93% for $Na_v1.4$ D1241I and 77% for $Na_v1.7$ I1410D.

Substitution H12A Decreases KIIIA Affinity by Increasing Dissociation Rate and Modifies Specificity. Substitution of His12 with an alanine severely reduced the affinity of the toxin for all native channel isoforms (Fig. 4B). This substitution increased the IC_{50} values for $Na_v1.2$ and $Na_v1.4$ by >2000-fold, whereas in contrast, the increase in IC_{50} for $Na_v1.7$ was only 133-fold (Fig. 4B). The resulting sequence of affinities for KIIIA-H12A was $Na_v1.2 > Na_v1.7 \gg Na_v1.4$. These drastic changes in affinity were not due to changes in k_{on} (2- –6-fold decreases) but rather to changes in k_{off}, 1.4 (700-fold increases), 30.4 (500-fold increase), and 2.0 min^{-1} (120-fold increase), for $Na_v1.2$, 1.4, and 1.7, respectively). Maximal block by KIIIA-H12A was slightly reduced in all three channels (to

TABLE 2

Kinetic analysis of KIIIA K7A binding (k_{on}) and unbinding (k_{off})

Fractional block at saturating toxin concentrations (Fb_{sc}) are determined from the dose-response curves in Fig. 3.

Channel	k_{on}	S.E.M.	k_{off}	S.E.M.	K_d	Fb_{sc}	S.E.M.
	$\mu M^{-1} \cdot min^{-1}$		min^{-1}		μM		
$Na_v1.2$	0.180	0.013	0.030	0.004	0.169	0.678	0.017
$Na_v1.4$	0.512	0.035	0.680	0.045	1.327	0.603	0.021
$Na_v1.7$	0.117	0.019	0.369	0.022	3.170	0.581	0.033
$Na_v1.4$ Y401F	0.441	0.027	0.445	0.042	1.011	0.687	0.017
$Na_v1.4$ D1241I	0.455	0.056	0.603	0.046	1.326	0.625	0.029

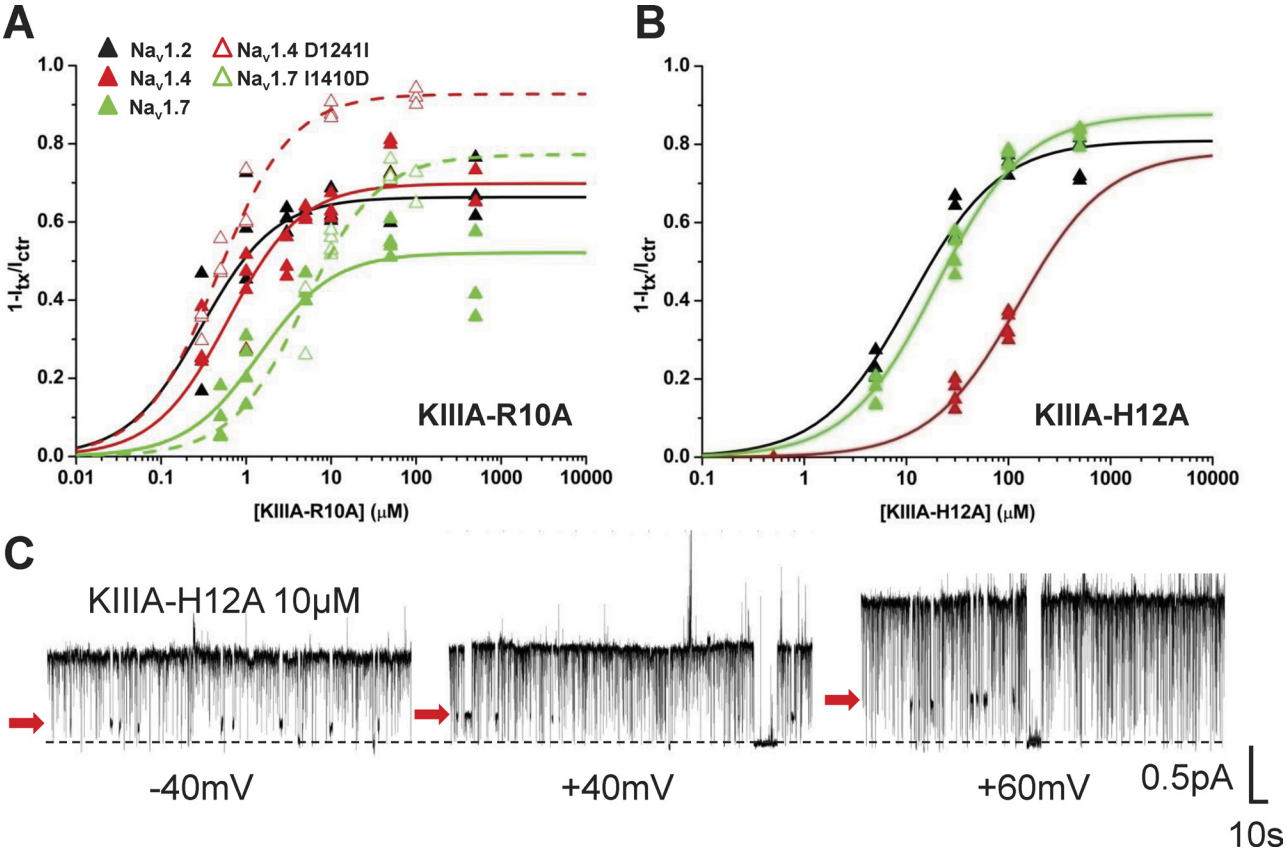

Fig. 4. Substitutions in KIIIA decrease maximal block (R10A), and binding affinity (H12A). A, dose-response curves for KIIIA-R10A (data from 89 cells) block of $Na_v1.2$, $Na_v1.4$, $Na_v1.7$, $Na_v1.4$ D1241I, and $Na_v1.7$ I1410D. Maximal block ranges from ~0.5 to ~0.9. B, dose-response curves of KIIIA-H12A (data from 89 cells) for $Na_v1.2$, $Na_v1.4$, and $Na_v1.7$. IC_{50} values are ~1000-fold larger than for KIIIA wt for the same channel isoforms. C, batrachotoxin-modified, single-channel currents showing KIIIA-H12A blocked levels (red arrow; black dotted line denotes fully closed level) of rat skeletal muscle sodium channels ($Na_v1.4$). Given the low affinity of H12A, it was not possible to use high enough concentrations to determine maximal block from whole-cell dose-response data; in the single-channel recordings, the blocked fraction, with H12A bound, was ~0.8. This value was used to constrain the fit of the dose-response curve for $Na_v1.4$ in B.

81% for $Na_v1.2$, 78% for $Na_v1.4$, and 88% for $Na_v1.7$). For $Na_v1.4$, given the very low affinity, the maximal block was estimated from single-channel recordings using lipid bilayers (Fig. 4C).

Binding of KIIIA Is Enhanced at Low pH Based on Increased Association Rates. To examine the effects protonation on KIIIA-wt block, we measured the kinetics of toxin binding and unbinding at pH 6.0, 7.4, and 9.0. An example of the effects of pH on KIIIA-wt block of $Na_v1.4$ is shown in Fig. 5A. Increasing the pH caused a decrease in k_{on} in $Na_v1.2$, 1.4, and 1.7 (Fig. 5C). For $Na_v1.2$, the k_{on} decreased from 2.2 $\mu M^{-1} \cdot min^{-1}$ at pH 6.0 to 0.28 $\mu M^{-1} \cdot min^{-1}$ at pH 7.4, and to 0.053 $\mu M^{-1} \cdot min^{-1}$ at pH 9.0. Similar to $Na_v1.2$, the channels $Na_v1.4$ and $Na_v1.7$ also showed decreases in k_{on} as the pH was increased (Fig. 5C). On average, across the three channel isoforms, k_{on} decreased 13-fold per pH unit over the pH range from 6.0 to 9.0.

The effects of pH on k_{off} were less pronounced (Fig. 5D). In $Na_v1.2$, there was no significant difference in k_{off} between pH 6.0 and 7.4 (0.004 and 0.002 min^{-1}, respectively), whereas $Na_v1.4$ showed a slight decrease in k_{off} from pH 6.0 to 7.4 (0.11 and 0.060 min^{-1}, respectively). However, from pH 6.0 or 7.4 to 9.0, both $Na_v1.2$ and $Na_v1.4$ showed an increase in k_{off} (to 0.010 and 0.43 min^{-1}, respectively). For $Na_v1.7$ there was no significant changes in k_{off} across all three pH values (0.012, 0.017, and 0.015 min^{-1}, respectively).

The strong influence of pH on k_{on}, combined with its minimal influence on k_{off}, resulted in a decreased affinity as pH increases. As a consequence, for KIIIA-wt block of $Na_v1.2$, the K_d increased by ~90-fold from 2 to 183 nM, from pH 6.0 to 9.0. Similar results were seen for $Na_v1.4$ and $Na_v1.7$ (Fig. 5E). Even in the absence of a free N-terminal amino group (see below), there is sufficient residual pH sensitivity to see a monotonic increase in K_d in the range of pH 6 to 9.

Removal of the Charged Amine at the KIIIA N terminus Strongly Attenuates pH Dependence. To learn the basis of the pH effects on k_{on}, we constructed a toxin derivative lacking the titratable N-terminal amino group desamino KIIIA (KIIIA-DA) and tested the effects of changes in pH on its kinetics (Fig. 5B, gray). There was a reduced sensitivity of k_{on} to pH for all the native channels (Fig. 5C). These changes, averaged over the three channel isoforms, reflect a decrease in k_{on} of 1.7-fold per pH unit (approximately 13-fold for KIIIA-wt) over the pH range from 6.0 to 9.0 (see above).

Similar to the effects of pH on wild-type KIIIA's k_{off}, pH has little effect on KIIIA-DA's k_{off}. In $Na_v1.2$, there was no significant difference in k_{off} across pH (0.025, 0.014, and 0.018 min^{-1} for pH 6.0, 7.4, and 9.0, respectively) (Fig. 5D). However, in both $Na_v1.4$ and $Na_v1.7$, there is a significant difference between pH 7.4 and 9.0 (0.10 and 0.48 min^{-1} for $Na_v1.4$ and 0.016 and 0.063 min^{-1} for $Na_v1.7$).

The reduced pH effect on KIIIA-DA's k_{on} compared with KIIIA-wt, leads to a smaller increase in K_d as pH is increased. In $Na_v1.2$, the K_d increases from 162 nM at pH 6.0 to 186 nM at pH 7.4 and to 635 nM at pH 9.0 (Fig. 5E). Similar to these results, $Na_v1.4$ and $Na_v1.7$ also increase in K_d from pH 6.0 to 7.4 to 9.0 (199 nM, 294 nM, and 3.2 μM for $Na_v1.4$ and 145 nM, 558 nM, and 5.5 μM for $Na_v1.7$, respectively).

Double Mutant Cycle Analysis and Molecular Dynamics Simulations of μ-CTX KIIIA-Bound Structure. The KIIIA structure was overlaid on the GIIIA docked conformation generated previously (Choudhary et al., 2007), and MD simulations were run for 20 ns. The toxin backbone was stable within an average root mean square deviation of 1.5Å. The largest cluster contained >60% of all the structures calculated. Its central structure is shown in Fig. 6A (green backbone), along with the starting structure (purple backbone). In this structure, Lys7 points toward the outer ring charges of domain I and II, whereas the Arg10 lies close to the domain I outer ring glutamate. Arg14 interacts with the outer ring charges in both domains III and IV, whereas the His12 lies between the outer ring charges of domains II and III.

We performed double mutant cycle analysis for toxin/channel pairs of KIIIA-Lys7 with $Na_v1.4$ Tyr401 and Asp1241, and for both KIIIA-Arg10 and KIIIA-Arg14 with $Na_v1.4$ Asp1241 and $Na_v1.7$ Ile1401 (Fig. 6D; Supplementary Table 1). KIIIA-Lys7 showed no substantial coupling to $Na_v1.4$ Tyr401 (0.27 kT), and only a small coupling (1.0 kT) to the outer ring domain III charge, $Na_v1.4$ Asp1241. The KIIIA-R10A and R14A derivatives both showed larger couplings than KIIIA-K7A, of 1.5 kT or greater, to the domain III outer ring charge ($Na_v1.4$ Asp1241). Experiments with $hNa_v1.7$ and its reciprocal outer ring mutation (I1410D) showed increased affinity for KIIIA-wt (Fig. 2E), whereas mutant cycle analysis showed similar or slightly greater coupling energies to those obtained with $rNa_v1.4$. Thus, these two sets of data confirm that residues Arg10 and Arg14 of KIIIA are both interacting partners with the domain III outer ring position on the channel.

Discussion

Differing Kinetics of KIIIA Block among Na_v Isoforms from Brain, Skeletal Muscle, and Peripheral Nerve. Wild-type KIIIA is selective among channel isoforms,

TABLE 3
Kinetic analysis of KIIIA R10A and H12A binding (k_{on}) and unbinding (k_{off})
Fractional block at saturating toxin concentrations (Fb_{sc}) is determined from dose-response data in Fig. 4.

Toxin (KIIIA) and Channel	k_{on}	S.E.M.	k_{off}	S.E.M.	K_d	Fb_{sc}	S.E.M.
	$\mu M^{-1} \cdot min^{-1}$		min^{-1}		μM		
R10A							
$Na_v1.2$	0.140	0.031	0.022	0.011	0.158	0.663	0.030
$Na_v1.4$	0.504	0.032	0.506	0.054	1.003	0.698	0.024
$Na_v1.7$	0.039	0.007	0.053	0.019	1.366	0.521	0.029
$Na_v1.4$ D1241I	0.206	0.032	0.088	0.005	0.428	0.927	0.019
$Na_v1.7$ I1410D	0.015	0.003	0.039	0.004	2.545	0.772	0.033
H12A							
$Na_v1.2$	0.129	0.025	1.392	0.115	10.791	0.809	0.021
$Na_v1.4$	0.275	0.101	30.388	4.114	110.497	0.780[a]	0[a]
$Na_v1.7$	0.106	0.016	2.035	0.123	19.282	0.877	0.019

[a] Maximal block was determined from the single-channel records in Fig. 4C.

as reflected by mean IC_{50} values for $Na_v1.2$ (5 nM, brain) over $Na_v1.4$ (37 nM, skeletal muscle) and $Na_v1.7$ (97 nM, peripheral nerve). Underlying the differences in affinity are changes in both binding and unbinding kinetics. The high affinity for $Na_v1.2$ is due predominantly to extremely slow dissociation (k_{off}, 0.002 min^{-1}), making it irreversible for

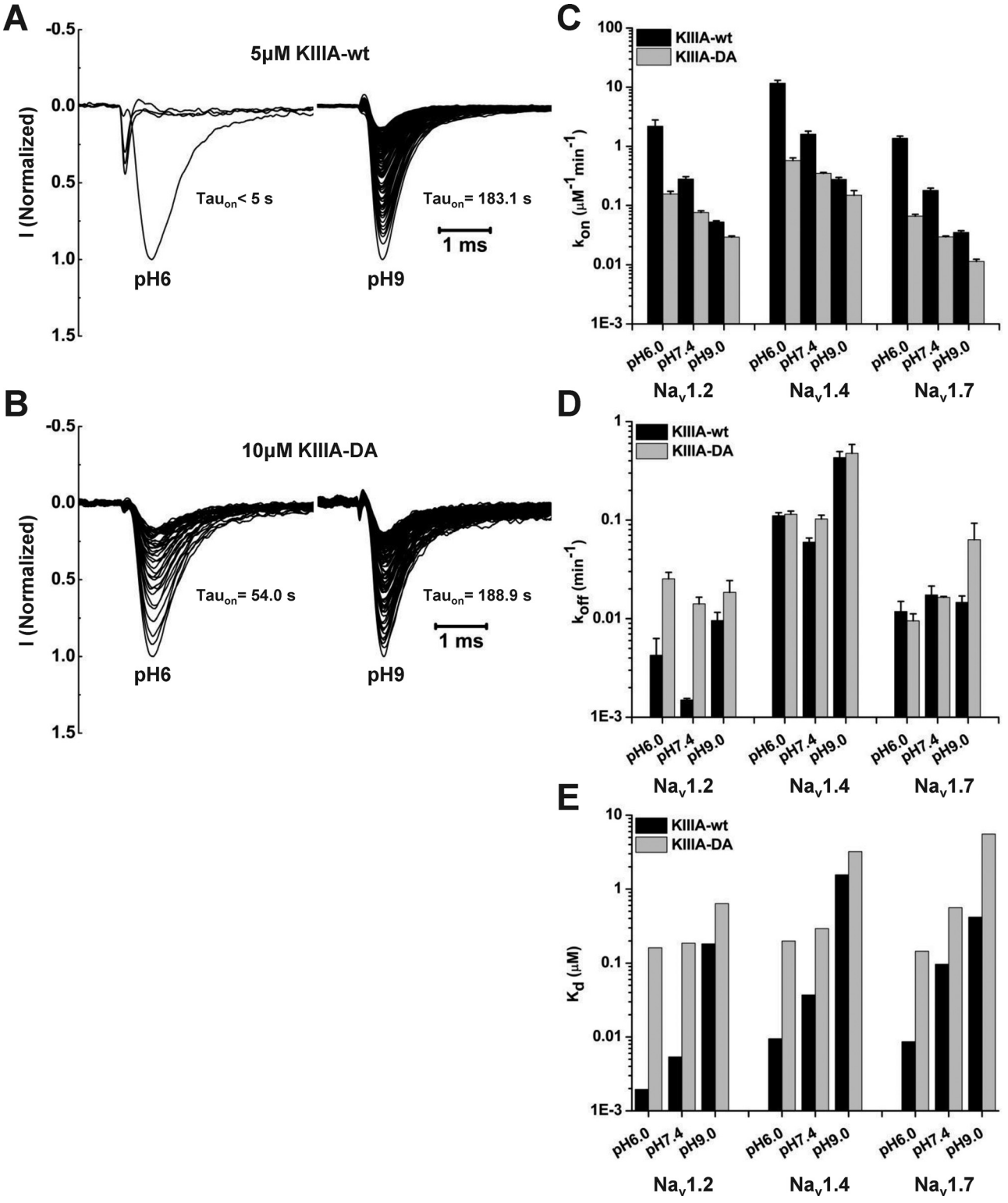

Fig. 5. Decreases in extracellular pH increase the affinity of KIIIA-wt by speeding up the association rate, largely because of protonation of the free N-terminal amine. Examples of current traces showing toxin wash-in at pH 6 and 9. Command voltage sequences were applied at 5-s intervals to elicit successive current traces. KIIIA-wt (5 μM) (A) and KIIIA-DA (10 μM) (B). At pH 6, note the much faster decrement in peak current for KIIIA-wt than for KIIIA-DA. C, k_{on} values for $Na_v1.2$, $Na_v1.4$, and $Na_v1.7$ at pH 6.0, 7.4, and 9.0. For 18 different experimental groups at different pHs and toxin concentrations, there was a total of 103 independent estimates of k_{on} and 68 estimates of k_{off}. D, values of k_{off} determined from the time courses of toxin washout. E, K_d values calculated as the ratios of mean values of k_{off} to k_{on}; see *Materials and Methods*.

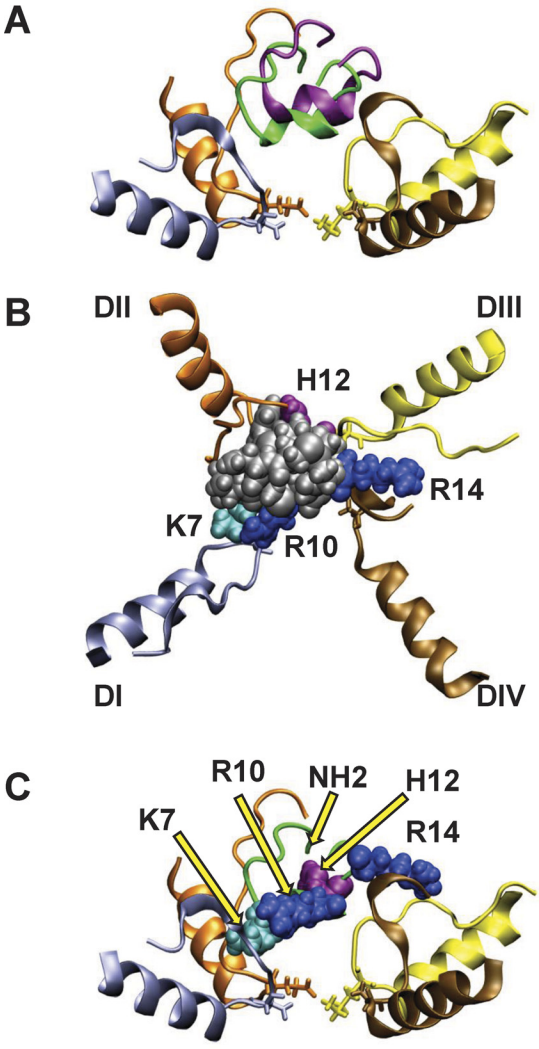

D

Coupling Energy (kT units)	$Na_v1.4$ Y401F	$Na_v1.4$ D1241I	$Na_v1.7$ I1410D
K7A	0.27	1.0	
R10A		1.5	2.5
R14A		1.8	1.7

Fig. 6. Molecular dynamics docking simulations and estimates of some toxin-channel coupling energies. A, starting (purple) and docked (green) structures of KIIIA with individually colored channel domains (domain I, ice blue; domain II, orange; domain III, yellow; domain IV, brown). B, space-filled docked structure of KIIIA, highlighting the amino acids studied. C, toxin backbone (green) with basic residues (space-filled) and with DEKA ring (liquorice stick format) residues highlighted. In the experiments, each of the toxin residues labeled, was either replaced by a neutral substitution, or titrated (-NH_2 terminal), to change the charge at that position. D, coupling energies, expressed as kT (where k is the Boltzmann constant and T is temperature in degrees Kelvin) and given as unsigned, absolute values, calculated from double mutant cycle analysis for interactions between toxin/channel residue pairs. The strongest couplings were found with channel domain III, pore outer ring position (see Fig. 1).

most practical purposes. $Na_v1.7$, another neuronal channel, shows k_{on} values similar to $Na_v1.2$ (0.18 versus 0.28 $\mu M^{-1} \cdot min^{-1}$, respectively) but the k_{off} for $Na_v1.7$ is approximately nine times faster (0.017 min^{-1}). $Na_v1.4$, a skeletal muscle channel, shows an intermediate IC_{50} but has the most divergent kinetics of the three. Its k_{on} is 6- to 9-fold faster (1.6 $\mu M^{-1} \cdot min^{-1}$) than those for both of the neuronal channels, but it also has the fastest k_{off} (0.060 min^{-1}). The faster kinetics in $Na_v1.4$ may reflect an evolutionary adaptation allowing the snail to rapidly immobilize its prey by blocking skeletal muscle action potentials (Table 1; Fig. 5C).

Compared with μCTX GIIIA and PIIIA, μCTX-KIIIA's higher affinities for both neuronal channels examined arise from a much slower dissociation rate. KIIIA's dissociation from $Na_v1.2$ is ~100-fold slower than that of PIIIA, whereas the association rate constants are not significantly different (McArthur et al., 2011a).

Derivative KIIIA-R14A Selectively blocks $Na_v1.7$, an Important Contributor to Pain Signaling. Unlike KIIIA-wt (affinities in the sequence $Na_v1.2 > 1.4 > 1.7$), KIIIA-R14A is selective for $Na_v1.7$ over both $Na_v1.2$ and $Na_v1.4$. The R14A substitution yielded a much less pronounced decrease in K_d for $Na_v1.7$ (~5-fold) than for $Na_v1.2$ (200-fold) and $Na_v1.4$ (150-fold), suggesting that 14 lacks the strong interaction with $Na_v1.7$ that occurs with both $Na_v1.2$ and $Na_v1.4$. Sequence alignment (Fig. 1A) shows this residue to be analogous to Arg19 in GIIIA and Arg20 in PIIIA. From MD docking simulations, we expected KIIIA-Arg14 to interact with the outer ring charges of domains III/IV for $Na_v1.2$ and $Na_v1.4$. However, the sequence alignment (Fig. 1B) shows that in $hNa_v1.7$, isoleucine replaces the outer ring aspartate that is present in domain III for both $Na_v1.2$ and $Na_v1.4$. The lack of this aspartate seems to account for the smaller change in affinity for $Na_v1.7$ associated with the KIIIA-R14A substitution.

The DIII outer ring reciprocal mutants (Fig. 1B) in $Na_v1.4$ D1241I and $Na_v1.7$ I1410D reveal a clear basis for the different affinities of KIIIA-wt for these two channels (Fig. 2E). The $Na_v1.4$ D1241I mutation increased the K_d to 102 nM, approximating that seen for $Na_v1.7$ (97 nM), whereas the reciprocal mutation ($Na_v1.7$ I1410D) mutation decreased the K_d to 56 nM, closer to that for $Na_v1.4$ (37 nM). Consistent with this, KIIIA-R14A showed very similar K_d values for the wild-type and mutant channel pairs (5.7 and 3.7 μM for $Na_v1.4$ and $Na_v1.4$ D1241I, versus 0.51 and 0.78 μM for $Na_v1.7$ and $Na_v1.7$ I1410D). This suggests that the DIII outer ring charge and Arg14 are interacting partners in toxin binding (see Fig. 6D and Supplementary Table 1 for coupling energies calculated from mutant cycle analysis).

Residues on Both Toxin and Channel Modulate Current through Toxin-Bound Channels. KIIIA-wt was the first native μCTX shown to allow a residual single channel current (5–10%) when the toxin is bound (Zhang et al., 2007). This current can be eliminated when guanidinium toxins such as tetrodotoxin or saxitoxin are applied after KIIIA is bound. Simultaneous binding of a KIIIA derivative and one of the guanidinium toxins modifies blocking and unblocking kinetics and opens a wider spectrum of pharmacological possibilities than the use of either type of toxin individually (Zhang et al., 2009; French et al., 2010).

The two KIIIA residues that strongly modulate maximal block (Lys7 and Arg10) are analogous to Arg14 and Lys17 in

PIIIA, where neutral substitutions enable similar residual currents (McArthur et al., 2011a). Furthermore, KIIIA-wt, which is six amino acids shorter than PIIIA, lacks a charged residue analogous to PIIIA-Arg12, suggesting that the observed residual current for KIIIA-wt could result from the lack of this charge.

KIIIA-K7A, shows the lowest degree of maximal block at saturating toxin concentrations, and this level is Na_v channel isoform-specific (Fig. 3A). From previous work, we expected Lys7 to interact with domain I and domain II between the inner and outer rings. Sequence alignment (Fig. 1B) shows a tyrosine adjacent to the inner ring for both $Na_v1.4$ and 1.7, in which $Na_v1.2$ has a phenylalanine. The mutation $Na_v1.4$ Y401F had little effect on the K_d of KIIIA-K7A but increased the maximal block to 69%, near that for $Na_v1.2$. This suggests that with KIIIA-K7A bound, ion passage through the channel is limited by Tyr401, which is a primary determinant of tetrodotoxin and saxiton affinity (Favre et al., 1995).

The KIIIA-R10A substitution also modulates maximal block. With R10A, maximal block is ordered as follows: $Na_v1.7<Na_v1.2<Na_v1.4$, likely as a result of the differences in domain III, where $Na_v1.7$ has an isoleucine, whereas $Na_v1.2$ and $Na_v1.4$ each have an aspartate.

The key new point here is that residues from both toxin and channel help to determine the toxin efficacy by controlling the maximal block. A full analysis of the chemical and steric factors involved will require extensive substitutions in both toxin and channel, taking advantages of general approaches developed earlier (Hui et al., 2002) and could reveal additional opportunities for pharmacological approaches using KIIIA derivatives in combination with other ligands (Zhang et al., 2009; French et al., 2010).

His12 of KIIIA Contributes Strongly to Binding to All Three Channel Isoforms. A conserved histidine (His12 in KIIIA) is found in μCTXs, which block both neuronal and skeletal muscle channels. In PIIIA, replacement of this residue by glutamine increased the affinity of PIIIA for skeletal muscle $Na_v1.4$ channels over neuronal $Na_v1.2$ (McArthur et al., 2011a). The KIIIA-H12A substitution severely reduced toxin affinity, primarily based dramatic increases in the dissociation rates (700-, 500-, and 120-fold increase in $Na_v1.2$, 1.4, and 1.7, respectively). This contrasts strongly with PIIIA, for which H19Q caused no reduction in affinity (McArthur et al., 2011a). KIIIA's smaller size and net charge may allow the histidine to play a more dominant role. The H12A-associated reductions in affinity were dramatic and result in preferential targeting of the two neuronal isoforms, $Na_v1.2$ and $Na_v1.7$, over skeletal muscle $Na_v1.4$ (Fig. 4B). Of the toxin derivatives that we studied, only H12A and R14A showed a clear change in channel isoform targeting preference from that of KIIIA-wt.

Protonation of KIIIA Increases Association Rate and Hence Affinity. Changing pH in the range of 6 to 9 produced obvious, systematic increases in k_{on} values as pH decreased, showing an average change of 13-fold per unit pH over the three channel subtypes, with little change in k_{off} (<3-fold). Thus, the large effect of the H12A substitution on dissociation rates rules out His12 as the primary mediator of pH effects. Furthermore, the parallel effects of pH on the three different channel isoforms make it unlikely that the major effect is mediated through titration of acidic residues in the channels' outer vestibules.

An alternate possibility is that a disulfide linkages in the toxin could be lost at higher pH. However, removal of only one of the three disulfide linkages yielded a lower k_{on} the C2–C15 linkage (Han et al., 2009; Khoo et al., 2009). This decrease in k_{on} fits with the KIIIA-wt pH results, the concomitant 10-fold increase in k_{off}, together with the rapid reversibility of our observed pH effects, makes disulfide bond disruption an unlikely rationale for our observations.

A third possibility is that KIIIA's free N terminus could be titrated by the changing pH, and indeed, this clearly affects the observed toxin kinetics. An examination of differences between the PIIIA and KIIIA structures supports this interesting possibility, because PIIIA block shows no dependence on pH (data not shown), and PIIIA lacks a free N-terminal charge as the residue is cyclized to form a pyroglutamate. Thus, we created a KIIIA derivative lacking the free N-terminal charge, KIIIA-DA. This derivative showed a reduced pH dependence from 13-fold to 1.7-fold change per pH unit. Consequently, the observed pH dependence of KIIIA block is due predominantly to titrating its free N-terminal charge, with the remaining dependence perhaps arising from the Asp11-His12 pair. This raises a possible complication for the strategy of toxin cyclization as a way of stabilizing the active conformation (Clark et al., 2010). If protonation of the free amino terminal were important for a pharmacological action, this option would be lost in the N-terminal to C-terminal cyclized version.

Possible Pharmacological Applications of KIIIA Derivatives. $Na_v1.7$ plays a role in pain signaling. Gain of function mutations lead to primary erythermalgia (Yang et al., 2004), whereas loss of function leads to congenital inability to experience pain (Cox et al., 2006; Fertleman et al., 2006), prompting a renewed interest in finding subtype selective blockers of $hNa_v1.7$. An interesting point is that numerous other species have a domain III outer ring aspartate instead of isoleucine, thus screening of $Na_v1.7$ modulators for human use that should use only $hNa_v1.7$. KIIIA has been shown previously to have analgesic behavior (Zhang et al., 2007). Further honing KIIIA targeting toward $hNa_v1.7$ poses a challenge, in that two substitutions that were found to enhance this targeting (H12A and R14A) substantially reduce KIIIA affinity.

Changes in pH in disease states are well documented. During ischemia, a drop of almost 1 pH unit has been observed (Kraig et al., 1983), and neuroprotective action of sodium channel blockers has been demonstrated (Carter et al., 2000). Thus, blocking toxins, whose affinity increases as pH decreases, may be well suited to combat such disease states.

Acknowledgments

We thank Dr. Gerald Zamponi for comments on a draft of the manuscript and Dr. Rocio Finol-Urdaneta for helpful discussions and suggestions. Structural coordinates for the KIIIA model were kindly provided by Drs. Brian Smith and Ray Norton (The Walter and Eliza Hall Institute of Medical Research, Parkville, VIC, Australia).

Authorship Contributions

Participated in research design: McArthur, Singh, Tieleman, and French.

Conducted experiments: McArthur.

Contributed new reagents or analytic tools: McArthur, McMaster, Winkfein, Tieleman, and French.

Performed data analysis: McArthur, Singh, and French.

Wrote or contributed to the writing of the manuscript: McArthur, Singh, McMaster, Winkfein, Tieleman, and French.

Performed stimulations: McArthur and Singh.

References

Al-Sabi A, McArthur J, Ostroumov V, and French RJ (2006) Marine toxins that target voltage-gated sodium channels. *Marine Drugs* **4:**157–192.

Berendsen HJ, Postma JPM, Vangunsteren WF, Dinola A, and Haak JR (1984) Molecular-dynamics with coupling to an external bath. *J Chem Physics* **81:**3684–3690.

Bulaj G, West PJ, Garrett JE, Watkins M, Marsh M, Zhang MM, Norton RS, Smith BJ, Yoshikami D, and Olivera BM (2005) Novel conotoxins from *Conus striatus* and *Conus kinoshitai* selectively block TTX-resistant sodium channels. *Biochemistry* **44:**7259–7265.

Cannon SC (1997) From mutation to myotonia in sodium channel disorders. *Neuromuscul Disord* **7:**241–249.

Carter AJ, Grauert M, Pschorn U, Bechtel WD, Bartmann-Lindholm C, Qu Y, Scheuer T, Catterall WA, and Weiser T (2000) Potent blockade of sodium channels and protection of brain tissue from ischemia by BIII 890 CL. *Proc Natl Acad Sci USA* **97:**4944–4949.

Catterall WA, Goldin AL, and Waxman SG (2005) International Union of Pharmacology. XLVII. Nomenclature and structure-function relationships of voltage-gated sodium channels. *Pharmacol Rev* **57:**397–409.

Choudhary G, Aliste MP, Tieleman DP, French RJ, and Dudley SC, Jr. (2007) Docking of mu-conotoxin GIIIA in the sodium channel outer vestibule. *Channels* **1**:344–352.

Clark RJ, Akcan M, Kaas Q, Daly NL, and Craik DJ (2010) Cyclization of conotoxins to improve their biopharmaceutical properties. *Toxicon* doi:10.1016/j.toxicon.2010.12.003.

Cox JJ, Reimann F, Nicholas AK, Thornton G, Roberts E, Springell K, Karbani G, Jafri H, Mannan J, Raashid Y, et al. (2006) An SCN9A channelopathy causes congenital inability to experience pain. *Nature* **444:**894–898.

Cruz LJ, Gray WR, Olivera BM, Zeikus RD, Kerr L, Yoshikami D, and Moczydlowski E (1985) *Conus geographus* toxins that discriminate between neuronal and muscle sodium channels. *J Biol Chem* **260:**9280–9288.

Cummins TR, Aglieco F, and Dib-Hajj SD (2002) Critical molecular determinants of voltage-gated sodium channel sensitivity to mu-conotoxins GIIIA/B. *Mol Pharmacol* **61:**1192–1201.

Daura X, Gademann K, Jaun B, Seebach D, van Gunsteren WF, and Mark AE (1999) Peptide folding: when simulation meets experiment. *Angew Chem Int Ed Engl* **38:**236–240.

Escayg A, MacDonald BT, Meisler MH, Baulac S, Huberfeld G, An-Gourfinkel I, Brice A, LeGuern E, Moulard B, Chaigne D, et al. (2000) Mutations of SCN1A, encoding a neuronal sodium channel, in two families with GEFS+2. *Nat Genet* **24:**343–345.

Favre I, Moczydlowski E, and Schild L (1995) Specificity for block by saxitoxin and divalent cations at a residue which determines sensitivity of sodium channel subtypes to guanidinium toxins. *J Gen Physiol* **106:**203–229.

Fertleman CR, Baker MD, Parker KA, Moffatt S, Elmslie FV, Abrahamsen B, Ostman J, Klugbauer N, Wood JN, Gardiner RM, et al. (2006) SCN9A mutations in paroxysmal extreme pain disorder: allelic variants underlie distinct channel defects and phenotypes. *Neuron* **52:**767–774.

French RJ, Yoshikami D, Sheets MF, and Olivera BM (2010) The tetrodotoxin receptor of voltage-gated sodium channels–perspectives from interactions with micro-conotoxins. *Mar Drugs* **8:**2153–2161.

Han TS, Zhang MM, Walewska A, Gruszczynski P, Robertson CR, Cheatham TE 3rd, Yoshikami D, Olivera BM, and Bulaj G (2009) Structurally minimized mu-conotoxin analogues as sodium channel blockers: implications for designing conopeptide-based therapeutics. *Chem Med Chem* **4:**406–414.

Hildebrand ME, Smith PL, Bladen C, Eduljee C, Xie JY, Chen L, Fee-Maki M, Doering CJ, Mezeyova J, Zhu Y, et al. (2011) A novel slow-inactivation-specific ion channel modulator attenuates neuropathic pain. *Pain* **152:**833–843.

Hille B (2001) *Ion Channels of Excitable Membranes,* Sinauer Assoc. Inc., Sunderland, Massachusetts.

Hui K, Lipkind G, Fozzard HA, and French RJ (2002) Electrostatic and steric contributions to block of the skeletal muscle sodium channel by mu-conotoxin. *J Gen Physiol* **119:**45–54.

Humphrey W, Dalke A, and Schulten K (1996) VMD: visual molecular dynamics. *J Mol Graph* **14:**33–38, 27–28.

Khoo KK, Feng ZP, Smith BJ, Zhang MM, Yoshikami D, Olivera BM, Bulaj G, and Norton RS (2009) Structure of the analgesic mu-conotoxin KIIIA and effects on the structure and function of disulfide deletion. *Biochemistry* **48:**1210–1219.

Kraig RP, Ferreira-Filho CR, and Nicholson C (1983) Alkaline and acid transients in cerebellar microenvironment. *J Neurophysiol* **49:**831–850.

Li RA, Ennis IL, Tomaselli GF, French RJ, and Marbán E (2001) Latent specificity of molecular recognition in sodium channels engineered to discriminate between two "indistinguishable" mu-conotoxins. *Biochemistry* **40:**6002–6008.

Li RA, Ennis IL, Xue T, Nguyen HM, Tomaselli GF, Goldin AL, and Marbán E (2003) Molecular basis of isoform-specific micro-conotoxin block of cardiac, skeletal muscle, and brain Na+ channels. *J Biol Chem* **278:**8717–8724.

Lindahl E, Hess B, and van der Spoel D (2001) GROMACS 3.0: a package for molecular simulation and trajectory analysis. *J Mol Model* **7:**306–317.

Linford NJ, Cantrell AR, Qu Y, Scheuer T, and Catterall WA (1998) Interaction of batrachotoxin with the local anesthetic receptor site in transmembrane segment IVS6 of the voltage-gated sodium channel. *Proc Natl Acad Sci USA* **95:**13947–13952.

McArthur JR, Ostroumov V, Al Sabi A, McMaster D, and French RJ (2011a) Multiple, distributed interactions of mu-conotoxin PIIIA associated with broad targeting among voltage-gated sodium channels. *Biochemistry* **50:**116–124.

McArthur JR, Singh G, O'Mara ML, McMaster D, Ostroumov V, Tieleman DP, and French RJ (2011b) Orientation of mu-conotoxin PIIIA in a sodium channel vestibule, based on voltage dependence of its binding. *Mol Pharmacol* **80:**219–227.

Santarelli VP, Eastwood AL, Dougherty DA, Horn R, and Ahern CA (2007) A cation-pi interaction discriminates among sodium channels that are either sensitive or resistant to tetrodotoxin block. *J Biol Chem* **282:**8044–8051.

Shon KJ, Olivera BM, Watkins M, Jacobsen RB, Gray WR, Floresca CZ, Cruz LJ, Hillyard DR, Brink A, Terlau H, et al. (1998) mu-Conotoxin PIIIA, a new peptide for discriminating among tetrodotoxin-sensitive Na channel subtypes. *J Neurosci* **18:**4473–4481.

Trimmer JS, Cooperman SS, Tomiko SA, Zhou JY, Crean SM, Boyle MB, Kallen RG, Sheng ZH, Barchi RL, and Sigworth FJ (1989) Primary structure and functional expression of a mammalian skeletal muscle sodium channel. *Neuron* **3:**33–49.

Wang Q, Shen J, Splawski I, Atkinson D, Li Z, Robinson JL, Moss AJ, Towbin JA, and Keating MT (1995) SCN5A mutations associated with an inherited cardiac arrhythmia, long QT syndrome. *Cell* **80:**805–811.

Waxman SG, Dib-Hajj S, Cummins TR, and Black JA (1999) Sodium channels and pain. *Proc Natl Acad Sci USA* **96:**7635–7639.

Yang Y, Wang Y, Li S, Xu Z, Li H, Ma L, Fan J, Bu D, Liu B, Fan Z, et al. (2004) Mutations in SCN9A, encoding a sodium channel alpha subunit, in patients with primary erythermalgia. *J Med Genet* **41:**171–174.

Zhang MM, Green BR, Catlin P, Fiedler B, Azam L, Chadwick A, Terlau H, McArthur JR, French RJ, Gulyas J, et al. (2007) Structure/function characterization of micro-conotoxin KIIIA, an analgesic, nearly irreversible blocker of mammalian neuronal sodium channels. *J Biol Chem* **282:**30699–30706.

Zhang MM, McArthur JR, Azam L, Bulaj G, Olivera BM, French RJ, and Yoshikami D (2009) Synergistic and antagonistic interactions between tetrodotoxin and mu-conotoxin in blocking voltage-gated sodium channels. *Channels* **3:**32–38.

Address correspondence to: Dr. Robert J. French, Physiology and Pharmacology, University of Calgary, 3330 Hospital Drive NW, Calgary, AB T2N 4N1, Canada. E-mail: french@ucalgary.ca